

Estimation of wind drift current in the Soya Strait

Wei Zhang¹ · Naoto Ebuchi² · Yasushi Fukamachi² · Yutaka Yoshikawa³

Received: 26 May 2015 / Revised: 21 October 2015 / Accepted: 1 November 2015 / Published online: 23 November 2015
© The Oceanographic Society of Japan and Springer Japan 2015

Abstract Three high-frequency (HF) ocean radars were deployed around the Soya (La Pérouse) Strait in 2003 to monitor the Soya Warm Current (SWC). Surface current observed by the HF radars contains a wind drift component, which must be removed in order to estimate the interior SWC. The wind drift parameters, speed factor and turning angle were derived from the surface current measured by the HF radars, the vertical current profile measured by a bottom-mounted acoustic Doppler current profiler (ADCP), and wind data from the numerical weather analysis system operated by the Japan Meteorological Agency (JMA) from October 1, 2006 to July 24, 2008. The ensemble-mean turning angle and speed factor from the entire dataset (excluding August 2007) were estimated to be 28° and 0.66 %, respectively. No significant seasonal variations were discernible in the wind drift parameters. After removal of the wind drift current estimated from the wind with the ensemble-mean drift parameters, the correlation coefficient between the along-shore current speed and sea level difference between the Sea of Japan and Sea of Okhotsk improved from 0.791 to 0.825. It was revealed that the magnitude of wind drift current reaches 45 % of that of the interior current in winter and approximately 20 %

in summer, indicating the importance of wind drift current estimation in this region.

Keywords High-frequency ocean radar · Wind drift current · Soya warm current · Acoustic Doppler current profiler · Soya Strait · Interior current

1 Introduction

The Soya (La Pérouse) Strait is a narrow and shallow strait located between Hokkaido Island, Japan and Sakhalin Island, Russia (Fig. 1). It is the main passage connecting the Sea of Japan and Sea of Okhotsk. The Soya Warm Current (SWC) flows through the Soya Strait from the Sea of Japan to the Sea of Okhotsk and plays an important role in the water mass exchange between the two seas. The surface current velocity and volume transport of the SWC show significant seasonal variations due to the driving force of sea level difference between the Seas of Japan and Okhotsk (Ohshima 1994; Ebuchi et al. 2006, 2009; Nakanowatari and Ohshima 2014; among others). In order to continuously monitor the spatial structures and temporal variations of the SWC, three HF ocean radars were deployed around the Soya Strait in 2003. Ebuchi et al. (2006) described these HF ocean radars in detail. They showed that surface current velocity observed by the HF radars agrees well with in situ measurements by drifting buoys and shipboard acoustic Doppler current profilers (ADCPs). The observed surface current velocity of the SWC is as strong as 1 m s^{-1} in summer but becomes weak in winter. It was also confirmed that the surface current of the SWC is highly correlated with the sea level difference between the two seas. Fukamachi et al. (2008, 2010) estimated the volume transport of the SWC by combining the surface current data from the HF radars

✉ Wei Zhang
zhangwei@lowtem.hokudai.ac.jp

¹ Graduate School of Environmental Science, Hokkaido University, Sapporo, Japan

² Institute of Low Temperature Science, Hokkaido University, Sapporo, Japan

³ Graduate School of Science, Kyoto University, Kyoto, Japan

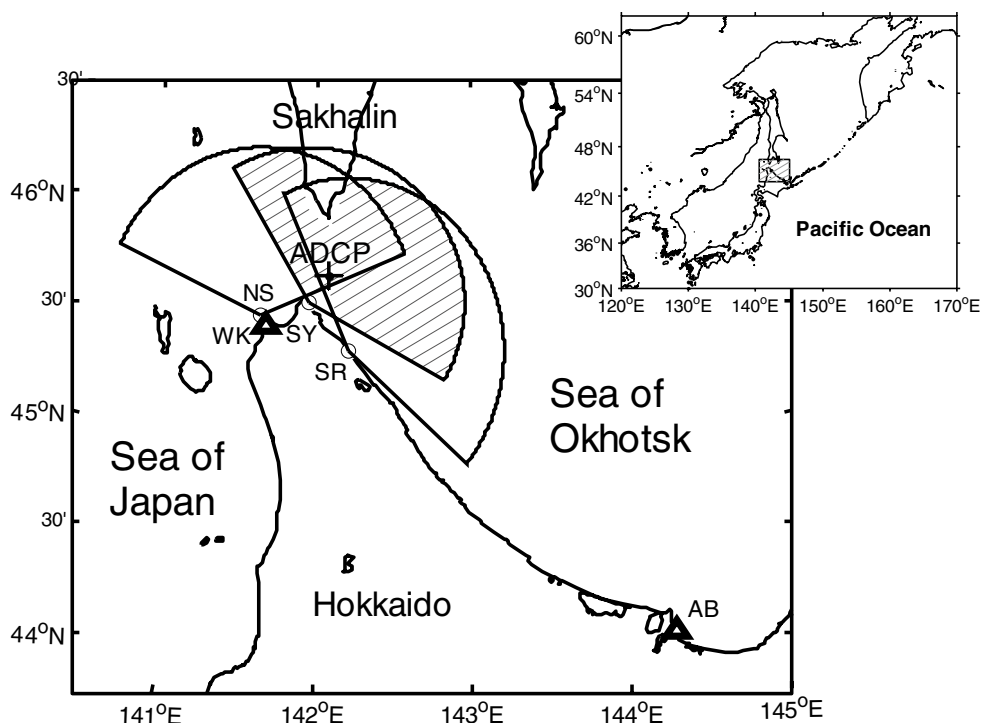


Fig. 1 Map of the Soya Strait and the surrounding area showing the coverage of the HF ocean radar stations (circles; NS Noshappu, SY Soya, SR Sarufutsu), locations of the tide-gauge stations (triangles;

WK Wakkanai, AB Abashiri), and bottom-mounted ADCP (cross). Two-dimensional surface current data are obtained in the *hatched* area. The *inset* map shows the location of the enlarged map

with the vertical current profile measured by a bottom-mounted ADCP.

The HF ocean radars measure the surface current velocity by using the Doppler shift of the radar frequency. In the case of the 13.9-MHz radars installed around the Soya Strait, the Doppler shift reflects the current velocity in the surface layer down to 1.72 m. Therefore, the surface current observed by the HF radars contains the wind drift component in addition to the interior component of the SWC. The wind drift and tidal current components must be removed in order to estimate the intensity of the interior SWC.

Numerous studies have been conducted on the basis of observations to reveal the structure of the surface Ekman layer (e.g., Weller 1981; Price et al. 1986, 1987; Schudlich and Price 1998; Yoshikawa et al. 2007). Due to wind variability and surface stratification, the assumptions of temporally stationary wind and vertically constant eddy viscosity are not always valid in the real ocean. In addition, Langmuir circulation and Stoke drift also affect the surface current. To estimate wind drift current caused by vector wind over the sea surface, a simple method based on the speed factor, which is defined as the ratio between the magnitudes of wind drift current and wind speed (or friction velocity), and turning angle, which is the difference between the directions of wind and wind drift current, has conventionally been utilized in practical applications (e.g.,

Tokeshi et al. 2007; Fukamachi et al. 2008, 2010; Ebuchi et al. 2009; Yoshikawa et al. 2010). However, the speed factor and turning angle are not universal; instead they change with various conditions such as wind variability and stratification in the surface boundary layer. Yoshikawa and Masuda (2009) derived the geostrophic current as the reference current to isolate the wind drift current from surface current measured by HF ocean radars and estimated wind drift parameters in the Tsushima (Korea) Strait. Although the Tsushima and Soya straits are the main passages of the Tsushima Warm Current (TWC) system, the Soya Strait is very narrow (40 km) and shallow (<55 m) compared with the Tsushima Strait (more than 100 km wide and approximately 110 m deep in the eastern channel). In the Soya Strait, the East Asian monsoon is strong and reinforces the wind drift current during winter, but the wind is weak and unstable during summer. These differences may result in the different wind drift parameters in the two straits. The wind drift parameters derived by Yoshikawa and Masuda (2009) in the Tsushima Strait are not likely applicable in the Soya Strait.

In this paper, we estimate wind drift parameters in the Soya Strait by the two methods described below. Then, we derive wind drift current from wind with these drift parameters and remove it from the surface current measured by the radars to obtain the interior SWC. Data used in

this study are described in Sect. 2, and the two methods to derive wind drift parameters are explained in Sect. 3. The derived wind drift parameters and their control factors are discussed in Sect. 4. The wind drift current is derived in Sect. 5. Finally, conclusions are given in Sect. 6.

2 Data and processing

2.1 HF radar data

Three SeaSonde HF ocean radars manufactured by CODAR Ocean Sensors were used to measure surface current in the Soya Strait (NS, SY, and SR in Fig. 1). The central frequency of these radars is 13.946 MHz, and the resolutions of current velocity, bearing angle, and range are $2.25 \times 10^{-2} \text{ m s}^{-1}$, 5° , and 3 km, respectively. Two-dimensional vector current data with an interval of 1 h were obtained in the hatched area in Fig. 1. Ebuchi et al. (2006) showed that radar data agree well with in situ current measurements made by drifting buoys and shipboard ADCPs. However, radio frequency interference (RFI) becomes intensive in summer and introduces occasional anomalous signals in the HF radar data. We conjecture that effects of the ionosphere on the reflection and absorption of the HF radio waves have clear seasonal variations, while activities of the RFI source may also vary seasonally. Therefore, additional quality control was applied to ensure the accuracy of the radar data.

In this study, the HF radar currents at the grid point closest to the ADCP site (in Fig. 1 within 0.1 km) were compared with the near-surface ADCP currents at a depth of 7.4–9.4 m to identify outliers contaminated by RFI (Fig. 2a). There exist data points with large differences. The radar data were removed when the differences between these two currents exceed 0.18 m s^{-1} in the zonal or 0.10 m s^{-1} in the meridional components for the entire period; then, linear interpolation was applied to fill gaps of up to 12 h in the time series. We chose the threshold values based on the root-mean-squared (RMS) differences between the HF radar measurements and in situ observations (Ebuchi et al. 2006). Figure 2b shows the comparisons of radar and ADCP velocities in the zonal direction after the quality control including interpolation; the solid lines are derived by principal component analysis. The figure indicates that the radar data are mostly consistent with the ADCP data after the quality control. Bias (HF radar – ADCP) and RMS difference for the zonal component were improved by the quality control and interpolation from -0.091 and 0.348 m s^{-1} to -0.028 and 0.208 m s^{-1} , respectively. There are still data points with large deviation due to the linear interpolation to fill data gaps. Afterwards, the tidal components in the HF radar current data

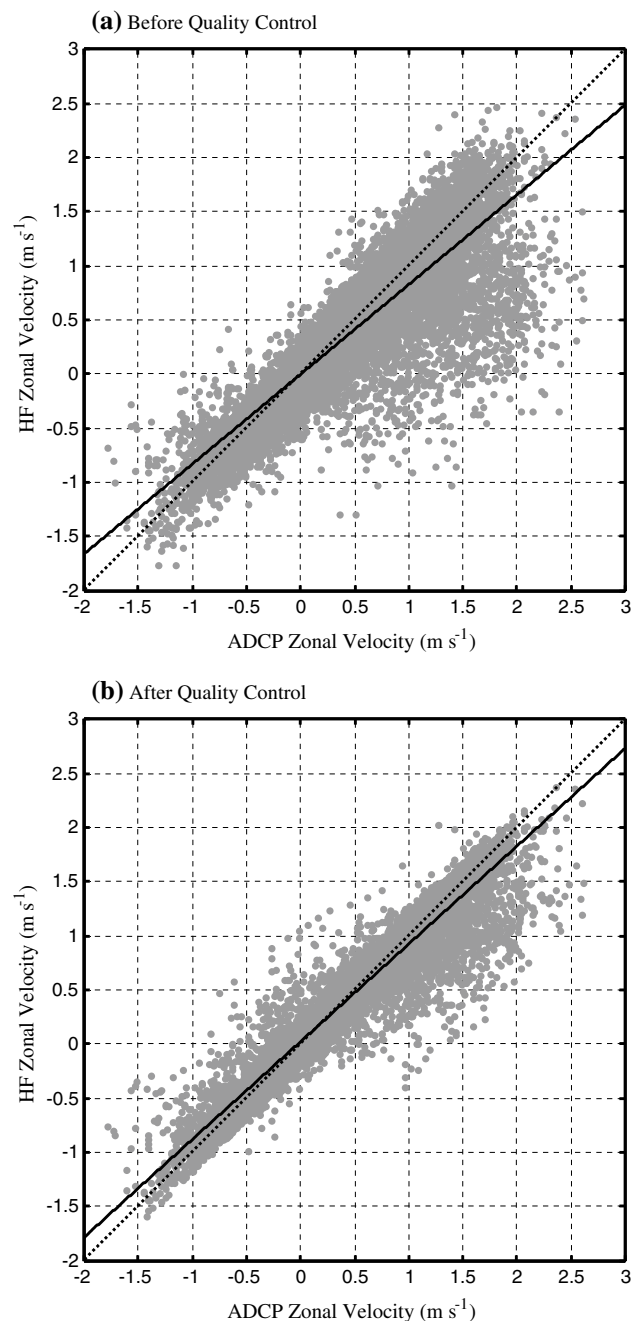


Fig. 2 Scatter plots of the hourly HF radar surface velocity and ADCP near-surface velocity in the zonal direction at a depth of 7.4–9.4 m **a** before and **b** after the quality control including the interpolation. *Solid lines* were obtained by principal component analysis. *Dotted lines* represent the one-to-one relationship

were removed by a 25-h running mean filter. A tide-killer filter (e.g., Thompson 1983; Hanawa and Mitsudera 1985), which requires a length of data for a period of 121 or 241 h, was not utilized to avoid larger data loss due to data gaps. We confirmed that the difference of the filters does not largely affect the results.

2.2 Bottom-mounted ADCP data

An ADCP (RD Instruments WH-Sentinel 300 kHz) was deployed about 18 km off the coast (142°4.7'E, 45°38.1'N), within the HF radar coverage in the middle of the Soya Strait where the water depth is about 51 m (cross in Fig. 1). To avoid damage due to fishing activities, the ADCP was housed in a trawl-resistant bottom mount (Flotation Technologies AL-200). The available measurements, from September 23, 2006 to July 24, 2008, captured the vertical current profiles in the Soya Strait with a 2-m bin interval from a depth of 45.4–47.4 to 3.4–5.4 m at a temporal interval of 1 h. Spikes in current velocity which exceeded 0.25 m s⁻¹ were removed. The tidal components in the ADCP data were eliminated by a 25-h running mean filter.

2.3 Wind data

Japan Meteorology Agency (JMA) provided meso-scale grid point values (GPV/MSM) of hourly operational weather-forecasting wind data at 10 m height, with a resolution of 0.05° in longitude and 0.0625° in latitude. In order to obtain the wind over the ADCP site, two-dimensional interpolation was applied to the data. Then, the time series of wind velocity were also smoothed with a 25-h running mean to match the current data.

2.4 Tide gauge data

It has been shown that the SWC is driven by the sea level difference between the Sea of Japan and Sea of Okhotsk (Ohshima 1994; Ebuchi et al. 2006, 2009; Matsuyama et al. 2006; among others). The sea level data obtained at two tide-gauge stations, Wakkanai and Abashiri (triangles labeled with WK and AB in Fig. 1), have been widely used to represent the sea levels in these two seas. For these tide-gauge data, the tide-killer filter designed by Hanawa and Mitsudera (1985) was applied to remove the tidal variations. A sea level pressure correction was carried out using data from the weather stations at Wakkanai and Abashiri.

3 Methods

3.1 Formulation

Wind drift current is induced by wind stress at the ocean surface. Due to the Coriolis effect, wind drift current flows to the right of wind direction in the northern hemisphere. In this study, wind drift current is described by wind speed as

$$\begin{pmatrix} u_w(x, y, t) \\ v_w(x, y, t) \end{pmatrix} = \alpha \begin{pmatrix} \cos \theta & \sin \theta \\ -\sin \theta & \cos \theta \end{pmatrix} \begin{pmatrix} U(x, y, t - \Delta t) \\ V(x, y, t - \Delta t) \end{pmatrix}, \quad (1)$$

where $[u_w(t), v_w(t)]$ is the wind drift current vector at time t , α is the speed factor, and θ is the turning angle between the wind and wind drift current (clockwise positive). (U, V) is the wind vector and Δt is the time lag between wind drift current and wind. u_w and v_w and U and V are along- and cross-shore components of wind drift current and wind, respectively. The along-shore component is 116° clockwise from north for the SWC at the ADCP location. The wind drift parameters, turning angle and speed factor, are assumed to be spatially uniform in the Soya Strait. To simplify the equation, we omit time t and position (x, y) , and rewrite Eq. (1) as

$$\begin{pmatrix} u_w \\ v_w \end{pmatrix} = \alpha \begin{pmatrix} \cos \theta & \sin \theta \\ -\sin \theta & \cos \theta \end{pmatrix} \begin{pmatrix} U(-\Delta t) \\ V(-\Delta t) \end{pmatrix}. \quad (2)$$

In this paper, we estimate the reference current by extrapolating the interior current, as described in Sect. 3.2. The surface wind drift current can be expressed as relative current, and is obtained by subtracting the reference current from the surface current, which is written as

$$\begin{pmatrix} u_{\text{rel}} \\ v_{\text{rel}} \end{pmatrix} = \begin{pmatrix} u_s \\ v_s \end{pmatrix} - \begin{pmatrix} u_{\text{ref}} \\ v_{\text{ref}} \end{pmatrix} = \begin{pmatrix} u_w \\ v_w \end{pmatrix} + \begin{pmatrix} u_{\text{res}} \\ v_{\text{res}} \end{pmatrix}, \quad (3)$$

where $(u_{\text{rel}}, v_{\text{rel}})$ is surface relative current, (u_s, v_s) is surface current, $(u_{\text{ref}}, v_{\text{ref}})$ is surface reference current, and $(u_{\text{res}}, v_{\text{res}})$ is the residue not correlated with the wind.

We use two methods to estimate wind drift parameters. The first method is the complex principal component analysis/empirical orthogonal function (PCA/EOF) method. Yoshikawa et al. (2007) applied the complex PCA/EOF method to estimate Ekman spiral from the first mode of the relative current. Here, we apply the complex PCA/EOF method to wind and surface relative current vectors, and estimate the wind drift parameters, namely, the turning angle and speed factor, from the calculated first mode of the relative current and wind.

In the second method, the wind drift parameters are estimated using the least squares method (LSM). Rewriting and expanding Eq. (3) gives

$$\begin{pmatrix} u_{\text{res}} \\ v_{\text{res}} \end{pmatrix} = \begin{pmatrix} u_{\text{rel}} \\ v_{\text{rel}} \end{pmatrix} - \begin{pmatrix} u_w \\ v_w \end{pmatrix} = \begin{pmatrix} u_s \\ v_s \end{pmatrix} - \begin{pmatrix} u_{\text{ref}} \\ v_{\text{ref}} \end{pmatrix} - \alpha \begin{pmatrix} \cos \theta & \sin \theta \\ -\sin \theta & \cos \theta \end{pmatrix} \begin{pmatrix} U(-\Delta t) \\ V(-\Delta t) \end{pmatrix}. \quad (4)$$

Yoshikawa and Masuda (2009) explained this method in detail. Unlike in Yoshikawa and Masuda (2009), we minimized $\sum[(u_{\text{res}})^2 + (v_{\text{res}})^2]$ instead of $\sum[(u_{\text{res}})^2]$ to calculate wind drift parameters, Σ means a summation over the time.

Since these two methods are independent, their results can be used to examine whether they each yield consistent wind drift parameters. Hereafter, these two methods will be denoted by CEOF and LSM.

3.2 Reference current

To calculate the wind drift parameters, we used the surface reference current to derive the surface relative current from the surface current, and regarded the surface relative current as the wind drift current in the calculations. Geostrophic current can be regarded as the reference current. Chereskin and Roemmich (1991) directly calculated the geostrophic current from hydrographic data as the reference current. Yoshikawa and Masuda (2009) derived the surface along-shore geostrophic current from the cross-shore sea level difference in the Tsushima Strait, and used this geostrophic current as the reference current. Also, interior current at a sufficient depth from the surface can be assumed as the reference current. Schudlich and Price (1998) chose interior currents at depths of 50 and 129 m as the reference currents in summer and winter, respectively. Yoshikawa et al. (2007) linearly extrapolated the shear of the interior current measured by an ADCP to the surface and used this extrapolated current as the reference current in the Tsushima Strait. In this study, it is not possible to derive the along-shore geostrophic current from the cross-shore sea level difference in the Soya Strait because the tide gauge data on the northern side (Sakhalin Island, Russia) are not available. Therefore, we followed the approach of Yoshikawa et al. (2007) to estimate the surface reference current by linearly extrapolating the shear of the interior current measured by the bottom-mounted ADCP deployed in the middle of Soya Strait (cross in Fig. 1).

The along-shore component of the interior current is closely related with the sea level difference between Wakkanai and Abashiri. Figure 3 shows correlation coefficients of the along-shore current and the sea level difference. The solid line indicates the correlations between the daily-mean along-shore velocity from each ADCP bin and the daily-mean sea level difference between Wakkanai and Abashiri. Horizontal bars denote lower and upper bounds for a 95 % confidence interval for each coefficient. We linearly extrapolated the current measured by the ADCP in an intermediate bin of 25.4–27.4 m to a near-surface layer bin of 3.4–5.4 m and extended it to the surface to define the reference current. Although we tried different depth ranges for the extrapolation, the results were not very different to the present case. We used a least squares linear fitting, based on the hourly data within a five-day window, to obtain the reference current on the middle day in the window (as shown in Fig. 4) and shifted the window by one day to get the reference current on the next day. The relative current was obtained by subtracting the surface reference current from the surface current measured by the HF ocean radars. The numbers of valid relative current in each month are shown in Fig. 5, and wind drift parameters are estimated from these data. Due to the RFI, there are fewer

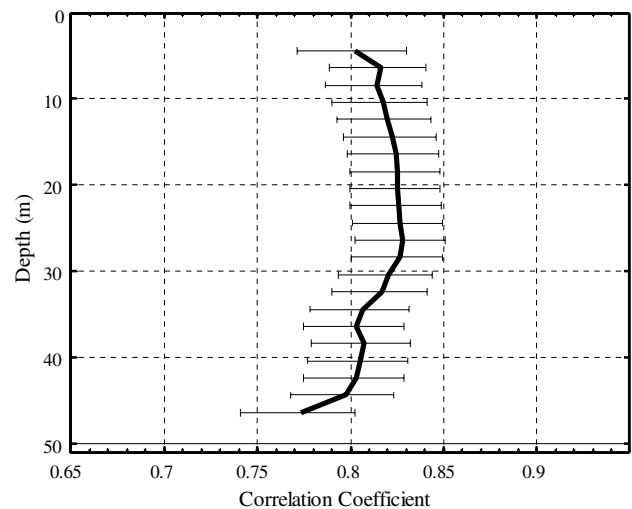


Fig. 3 Correlation coefficients between the daily-mean along-shore velocity from each ADCP bin and the daily-mean sea level difference between Wakkanai and Abashiri during the entire period. *Horizontal bars* denote lower and upper bounds of a 95 % confidence interval for each coefficient

data in summer. Although we tried applying parabolic and other fitting methods to the vertical current shear to obtain the reference current, the results did not show significant differences.

4 Estimation of drift parameters

4.1 Monthly-mean drift parameters

The wind drift parameters in each month, termed monthly-mean drift parameters, were calculated from the 22-month data using the two methods described in Sect. 3.1. The time lag, Δt in Eq. (4), was chosen as 12 h, as described in Sect. 4.2 below. The results of monthly-mean drift parameters are shown in Fig. 6. The turning angles estimated by the two independent methods, CEOF and LSM, are almost identical. The speed factors are roughly consistent (except in August and September 2007 due to small numbers of data). These results suggest that our estimations are robust. In August 2007, the turning angles have a negative value, indicating that the wind drift current flows to the left of the wind direction and are, thus, considered unrealistic. The negative turning angle seems to be mainly caused by statistical uncertainty due to the small number of data, and will be discussed in detail later in this section.

The monthly-mean turning angle varies from 3° to 64° across both methods, and the speed factor ranges from 0.29–1.29 % for the LSM and 0.57–1.97 % for CEOF method. For both methods, the mean turning angle was 29.7° , with a standard deviation (SD) of 16.2° . The mean

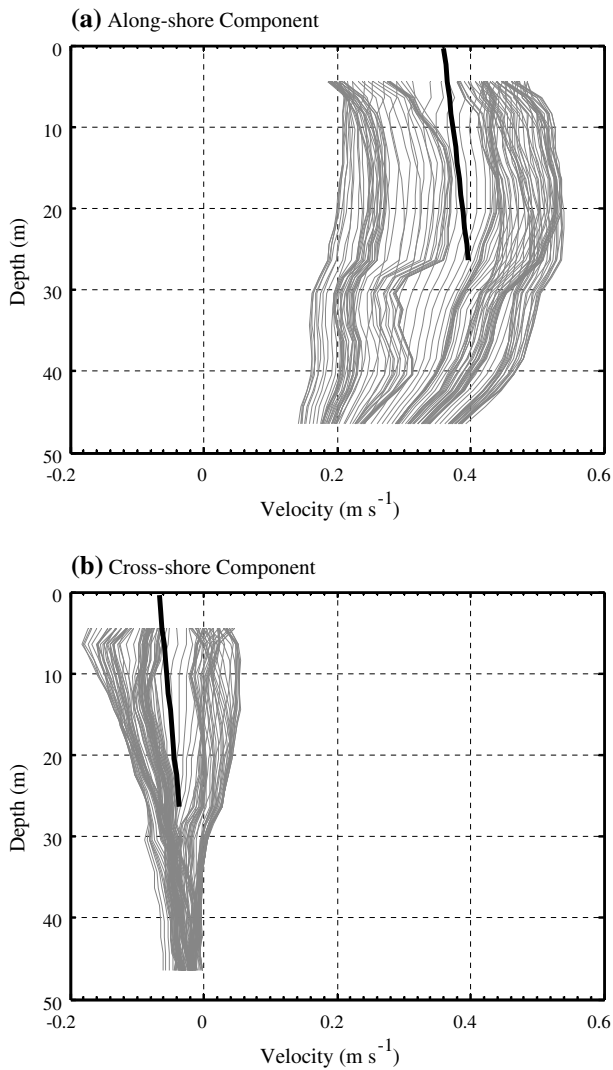


Fig. 4 Example of extrapolation used to estimate **a** along-shore and **b** cross-shore components of the reference current from the ADCP velocity in the upper bins. The data during June 11–15, 2007 were used to obtain the daily surface reference current on June 13, 2007

speed factor was 0.74 % with a SD of 0.35 % for the LSM, and 0.98 % with a SD of 0.43 % for the CEOF method. Although the speed factor and turning angle exhibited temporal variations, they did not show significant seasonal variations.

To investigate causes of the negative turning angle in August 2007, the root-mean-squared difference (RMSD) values between the along-shore components of the relative current (the HF radar surface current minus the surface reference current) and the wind drift current estimated from the wind using the turning angles and speed factors in Fig. 6 were calculated and are shown in Fig. 7. The RMSD value is quite large in August 2007 when the negative turning angle was calculated, implying that the estimation of the wind drift parameters is not reliable. A likely reason is

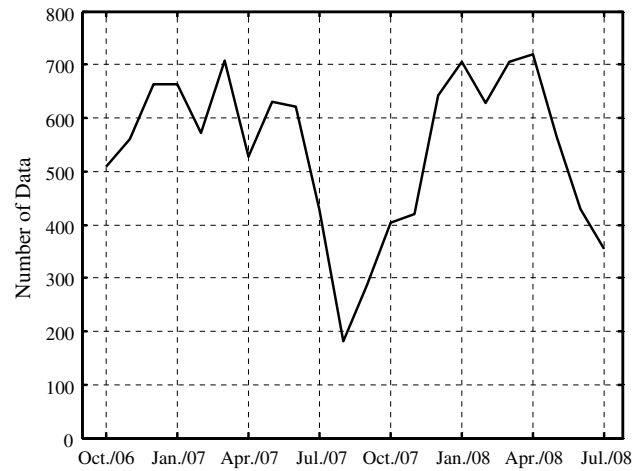


Fig. 5 Number of valid data used to calculate wind drift parameters in each month

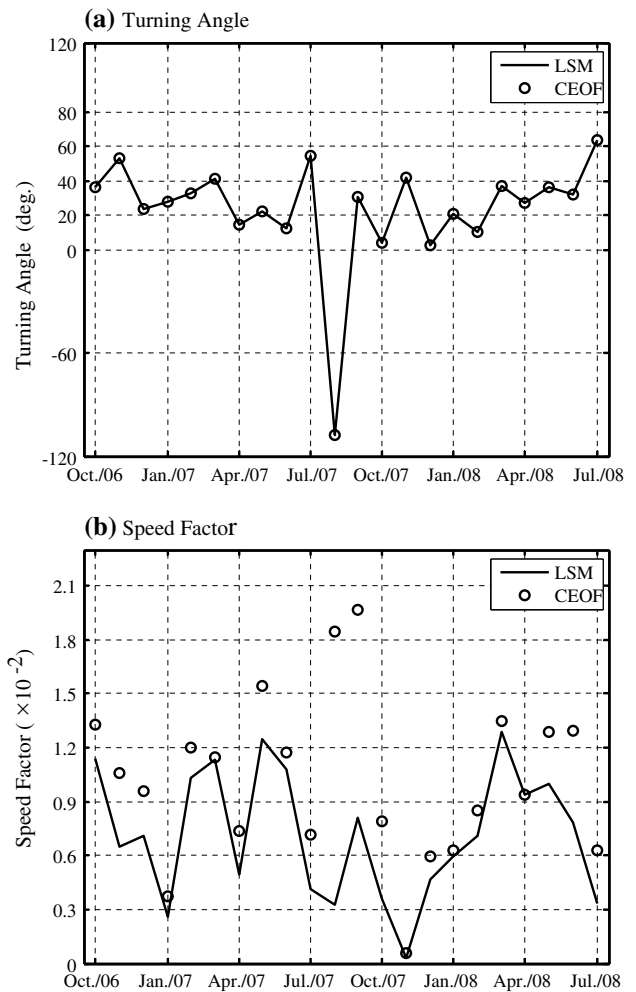


Fig. 6 Monthly-mean wind drift parameters, **a** turning angles and **b** speed factors, calculated by the two methods. Circles and lines denote the wind drift parameters calculated by the complex EOF (CEOF) and least squares methods (LSM), respectively

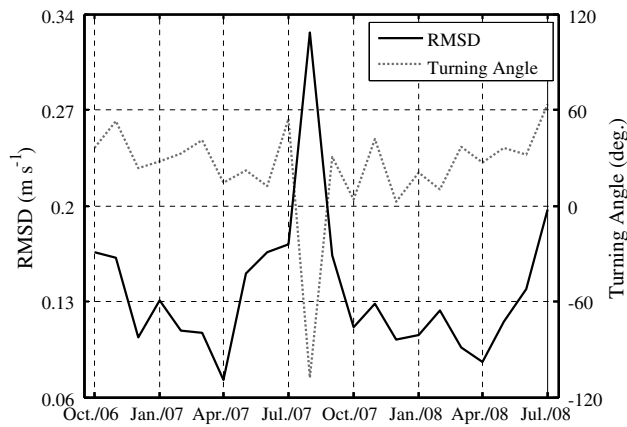


Fig. 7 Root-mean-squared differences (RMSDs) between the along-shore components of the relative current and wind drift current estimated by the LSM. The *black solid line* represents the RMSD values, and the *gray dotted line* represents the turning angles shown in Fig. 6a

that the number of data points (Fig. 5) is too small to yield a statistically accurate turning angle. Several other possible reasons for the negative turning angle are the weak wind with high variability in summer, the accuracy of the HF radar current measurements, and uncertainty in the reference current estimation, since the wind drift current is considered to be small under weak wind in summer and might be masked by the accuracy of the measurements and uncertainty in the reference current.

Figure 8 shows monthly-mean wind stability and wind speed with their SDs. Similar to the current stability in Hanawa et al. (1996), the wind stability is defined as the ratio of vector-averaged wind speed to scalar-averaged wind speed. This parameter can represent the variability in wind direction. If wind blows in one direction, the stability is one, and if wind direction rotates, the stability decreases towards zero. As expected, the wind direction is mainly unstable (stable) in spring and summer (fall and winter) and wind speed is weak (strong) in spring and summer (fall and winter) due to the northwesterly monsoon prevailing in fall and winter in this region. The weak and variable wind might be a factor resulting in the negative turning angle derived in the statistical analysis.

4.2 Time lag between the wind and wind drift current

The time lag between the wind drift current and wind is examined. Wind drift current was estimated from the wind, using the monthly-mean drift parameters calculated by the LSM and CEOF method with time lags of 0–25 h. Then, the wind drift current was removed from the along-shore surface current to derive the interior SWC. Correlation coefficients between the along-shore component of the

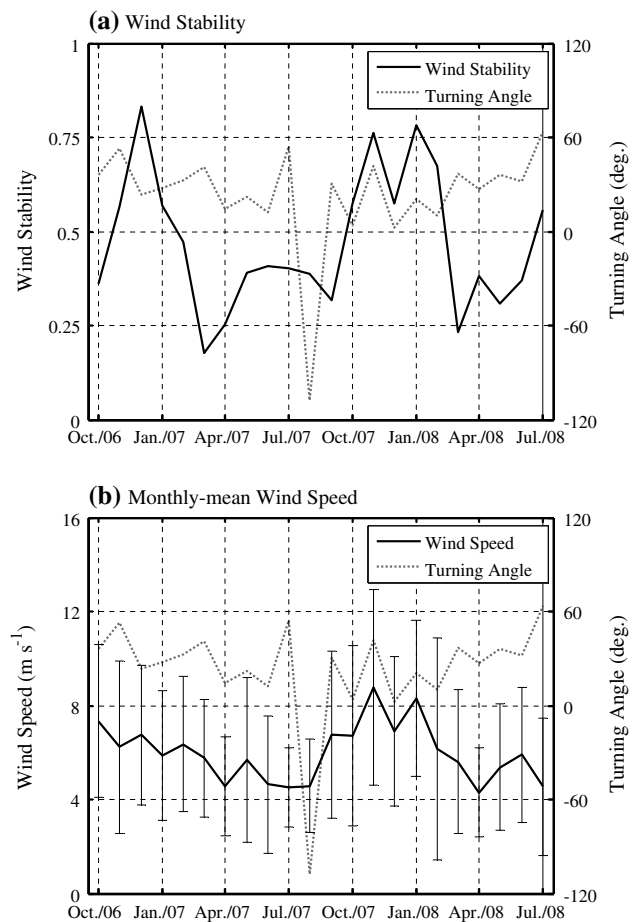


Fig. 8 a Wind stability and **b** mean wind speed in each month, shown by *black solid lines*. Turning angles calculated by the LSM are shown by the *gray dotted line*. *Vertical bars* denote the SD from the mean value in each month

interior SWC and the sea level difference between Wakkanai and Abashiri are shown in Fig. 9. The highest correlation was found at lags of 11 and 12 h for the LSM and CEOF methods, respectively. The time lag of 11–12 h is somewhat shorter than the inertial period of 17 h in this region. The wind drift parameters did not change appreciably for time lags of 6–24 h (not shown). Therefore, we chose a time lag (Δt) of 12 h in Eq. (4) in this study including the results shown above.

4.3 Seasonal variations

As shown in Fig. 6, seasonal variations in the wind drift parameters are not significant. We divided the 22-month data into 12 groups according to calendar month, and calculated the calendar-month-mean drift parameters using both methods. The calendar-month-mean drift parameters (solid line) calculated by the LSM are shown in Fig. 10. Data in August and September are available only in 2007,

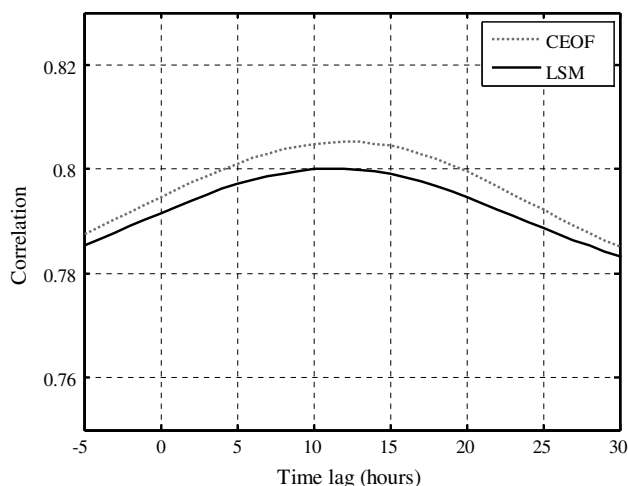


Fig. 9 Correlation coefficients between the sea level difference and the interior currents calculated by the two methods as a function of time lag between the wind and wind drift current. The peak is at 11 h for the LSM, and 12 h for the CEOF method. Positive time lags indicate that the wind leads the wind drift current

while those in the other months are available for 2 years. The wind drift parameters calculated by the CEOF method are roughly similar to those calculated by the LSM (not shown). Except for the turning angle outlier in August, the calendar-month-mean turning angle and speed factor vary by 15°–59° and 0.27–1.21 %, respectively, and do not show significant seasonal variations.

In the Tsushima Strait, Yoshikawa and Masuda (2009) reported clear seasonal variations in the wind drift parameters. Their results for a 3-day running mean are shown by the dotted line in Fig. 10. Large turning angles of 50.0°–67.8° and speed factors of 1.55–1.84 % in summer (June–August), and small turning angles of 15.8°–28.1° and speed factors of 0.98–1.17 % in winter (November–February), were derived. The values of the wind drift parameters in the Soya Strait are close to those in Tsushima Strait during winter. Yoshikawa and Masuda (2009) concluded that seasonal variations of wind drift parameters are likely caused by the net surface heat flux and density stratification. Using historical hydrographic data in the area of the Soya Strait (45°–46°N, 141°–143°E) from the Japan Oceanographic Data Center (JODC), we calculate the monthly-mean density, ρ_0 , and then obtain buoyancy stratification ($-g\Delta\rho/(\rho_0\Delta z)$) for depths of 0–10, 0–20, and 0–30 m (Fig. 11a), where g is the gravity acceleration, $\Delta\rho$ is the density difference between the specified depth and surface, and Δz is the depth. Also, using the data from the "Japanese Ocean Flux Data sets with Use of Remote Sensing Observations" study (J-OFURO2, Tomita et al. 2010) in the area of the Soya Strait (45.5°–46.5°N, 141.5°–142.5°E), we obtained monthly-mean net heat

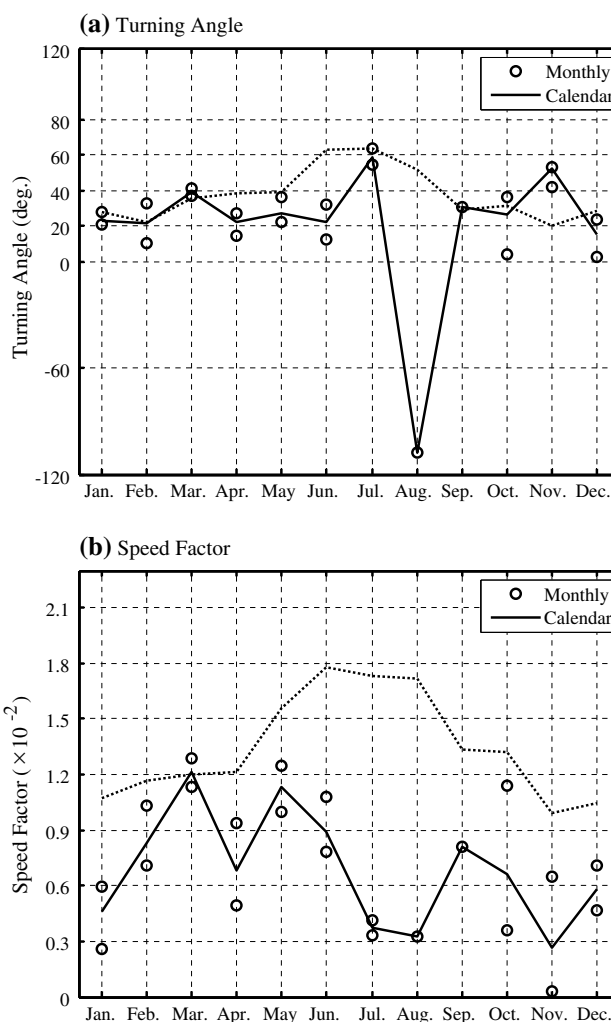


Fig. 10 Seasonal variations of the wind drift parameters calculated by the LSM in the Soya Strait: **a** turning angles and **b** speed factors. The black solid line is calendar-month-mean drift parameters (see the text for their definition), and the circles are the monthly-mean drift parameters. The dotted line represents the seasonal variation of the wind drift parameters in the Tsushima Strait (Yoshikawa and Masuda 2009)

flux (Fig. 11b). Both the density stratification and surface heat flux show significant seasonal variations. Amplitudes of the seasonal variations are similar to those reported by Yoshikawa and Masuda (2009) for the Tsushima Strait (see their Fig. 8). Therefore, values of the density stratification and surface heat flux, which are closely related to eddy viscosity, cannot explain the differences in the seasonal variations of wind drift parameters between the Soya and Tsushima straits.

The Soya Strait is shallower and narrower than the Tsushima Strait. We attempt to explore the effects of bottom and coastal boundary layers by following Yoshikawa and Masuda (2009). Typically, the vertical scale of the boundary layer, δ_E , for neutral stratification is estimated as

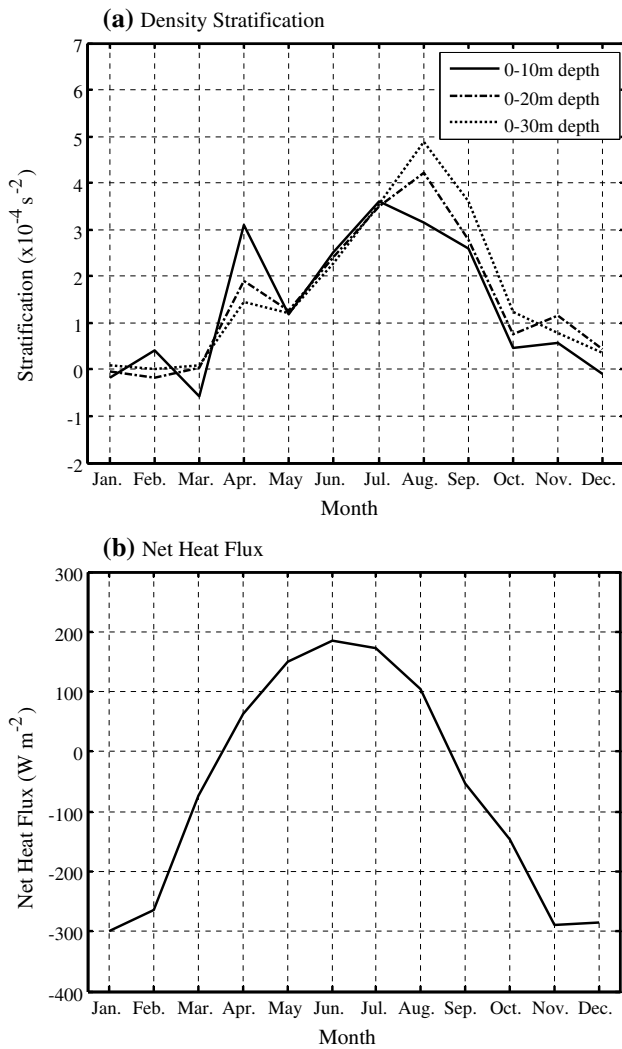


Fig. 11 **a** Monthly-mean density stratification near the surface over the region 45°–46°N and 141°–143°E at depths of 0–10, 0–20, and 0–30, and **b** monthly-mean surface net heat flux over the region 45.5°–46.5°N and 141.5°–142.5°E during 2006–2008

$$\delta_E \leq 0.4 \frac{u_*}{f}, \tag{5}$$

where u_* is the turbulent friction velocity of water and f is the Coriolis parameter (Cushman-Roisin 1994; Yoshikawa and Masuda 2009). With a typical value of $u_* = 0.01 \text{ m s}^{-1}$ (estimated using the formula by Toba 1988) and $f = 1 \times 10^{-4} \text{ s}^{-1}$ around the Soya Strait, δ_E is estimated to be $\leq 40 \text{ m}$, and can be comparable to the depth of the ADCP site (approximately 51 m). The correlation between the along-shore current and sea level difference shown in Fig. 3 decreases with depth from 26.4 to 46.4 m. This result also supports the bulk estimation of the bottom boundary layer. Therefore, the bottom boundary likely affects the surface boundary layer in the Soya Strait. In the Tsushima

Strait, Yoshikawa and Masuda (2009) ignored the bottom boundary effect because the water depth (110 m) is sufficiently deep.

The scale of the horizontal boundary layer, δ_H , is given by

$$\delta_H = \left(\frac{2A_H D}{f \delta_E} \right)^{1/2}, \tag{6}$$

where D is the depth of the strait and A_H is the horizontal eddy viscosity (Yoshikawa and Masuda 2009). Assuming $A_H = 200 \text{ m}^2 \text{ s}^{-1}$ (Teague et al. 2005) and $\delta_E \geq 2 \text{ m}$, we obtain δ_H as approximately 10 km, which is smaller than the distance from the ADCP site to the coast (about 18 km). Therefore, the horizontal boundary does not likely affect the wind drift current in the Soya Strait.

In contrast to the situation in the Tsushima Strait, the wind drift parameters in the Soya Strait did not show significant seasonal variations. Although we cannot currently present clear reasons for this difference, the difference in strait depths may be one of the possible factors. Ide and Yoshikawa (2015) found that the diurnal cycle of the surface heat flux may greatly affect the wind drift parameters. According to their results, the differences in the diurnal cycle between the Tsushima and Soya Straits could also be a possible reason. The estimation of the surface reference current by extrapolation using the vertical current profile (Sect. 3.2) could be greatly affected by the structures of the surface and bottom boundary layers in the Soya Strait. Also, various factors, such as differences in the wind variability and the mean current of the SWC and TWC, may contribute to the difference.

5 Wind drift current

5.1 Ensemble-mean wind drift parameters

As discussed in the previous section, the seasonal variations in the wind drift parameters are not significant. To estimate the wind drift current from the wind data for practical purposes, we calculated ensemble-mean drift parameters using all the data (except August 2007). The ensemble-mean turning angle and speed factor derived by the LSM are 28° and 0.66 %, respectively, and the ensemble-mean drift parameters derived by the CEOF method are 28° and 0.91 %, respectively. Previously, Fukamachi et al. (2008) estimated wind drift parameters based only on winter data from November 2004 to January 2005 at a different site (142°39.9'E, 45°15.5'N) near the Soya Strait, choosing the data in the uppermost ADCP bin as the surface reference current. Their turning angle and speed factor were 19° and 1.6 %, respectively. Fukamachi et al. (2010) also estimated

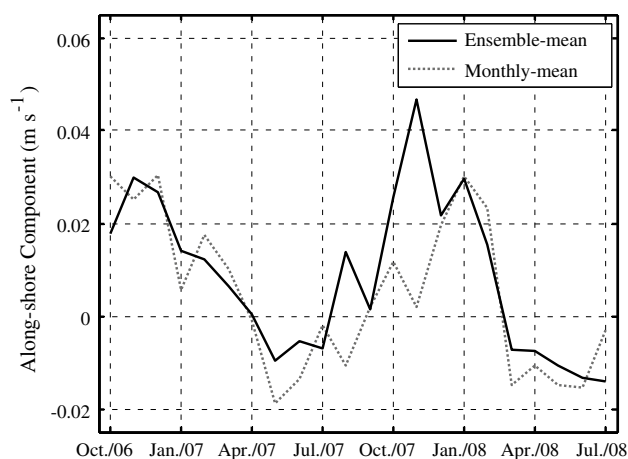


Fig. 12 Along-shore components of the wind drift currents estimated from the wind with the ensemble- (black solid line) and monthly-mean (gray dotted line) wind drift parameters by the LSM. Positive velocities indicate southeastward flows

wind drift parameters based on the data during the entire ADCP measurement period (as in the present study), choosing the data in an upper ADCP bin (7.4–9.4-m depth) as the surface reference current. Their wind drift parameters were 4.2° and 0.93% , respectively. The differences in locations, data periods, and definitions of the surface reference currents among these studies might affect the estimation of the wind drift parameters. However, we believe that our values are more reliable since the vertical shear of the interior current was considered in the estimation of the surface reference current, and because we utilized a longer period of data, even without the August 2007 data, when the values were questionable.

5.2 Analyses of wind drift currents

Using the estimated monthly- and ensemble-mean drift parameters, hourly along-shore wind drift currents were derived from wind data, and then monthly-mean wind drift currents were calculated from these hourly values. Figure 12 shows the along-shore components of wind drift current at the ADCP site estimated by the LSM using the monthly- and ensemble-mean drift parameters. The two wind drift currents generally agree with each other, except in August and November 2007. The difference in August 2007 is due to the negative monthly turning angle as described in Sect. 4.1. The difference in November 2007 is due to the nearly zero monthly speed factor (Fig. 6b), but we could not identify a specific reason for this small value. In spite of the difference between the monthly- and ensemble-mean drift parameters, the resultant wind drift currents are mostly similar, indicating that the ensemble-mean drift parameters are sufficient and effective for estimating the

wind drift current from wind in the Soya Strait. The seasonal variations in the wind drift current shown in Fig. 12 are mainly caused by the seasonal variations in the wind over the Soya Strait. Relatively strong southeastward wind drift currents exist in fall and early winter, and northwestward wind drift currents exist in spring and early summer.

The along-shore component of the SWC is closely related to the sea level difference between Wakkanai and Abashiri (e.g., Matsuyama et al. 2006; Ebuchi et al. 2006, 2009). The correlation coefficient of the daily-mean sea level difference between Wakkanai and Abashiri and the daily-mean along-shore current observed by the HF radars at the ADCP location for the entire data period from October 2006 to July 2008 is 0.791. We calculated the wind drift current using the ensemble-mean wind drift parameters by the LSM, and subtracted it from the along-shore surface current measured by the radars. In this case, the correlation coefficient increases to 0.825. The increase from 0.791 to 0.825 is confirmed to be statistically significant by the Steiger's paired t test (Steiger 1980), with a confidence level of 99 %.

Next, we examine spatial distributions of the wind and various currents. The interior current at the surface was obtained by subtracting the wind drift current from the surface current observed by the HF ocean radars. Figure 13 shows examples in January 2008. In winter, the East Asian monsoon is strong around the Soya Strait (Fig. 13a) and results in a sizable wind drift current (Fig. 13b). Comparison between the surface current measured by the HF ocean radars (Fig. 13c) and the interior current (Fig. 13d) clearly shows the influence of the wind drift current.

Figure 14 shows a monthly time series of the spatial-mean magnitude ratio of the wind drift current and interior current at the surface. The ratio was calculated within 50 km off the coast, which is a typical width of the SWC (Ebuchi et al. 2006). The ratio reaches 45 % in winter when the East Asian monsoon is strong while the interior SWC is weak. The ratio is even nearly 20 % in summer when the wind is weak while the interior SWC is strong. These examples shown in Figs. 13 and 14 exhibit the importance of the wind drift current estimation and the evaluation of the interior SWC from the data measured by the HF radars.

6 Summary

In the Soya Strait, the wind drift parameters, turning angle and speed factor were investigated using the surface current from the HF ocean radars, the sea level difference from coastal tide gauges, the wind data from the JMA/GPV/MSM, and the vertical current profile from a bottom-mounted ADCP. Monthly- and ensemble-mean wind drift parameters were calculated from the 22-month data by the

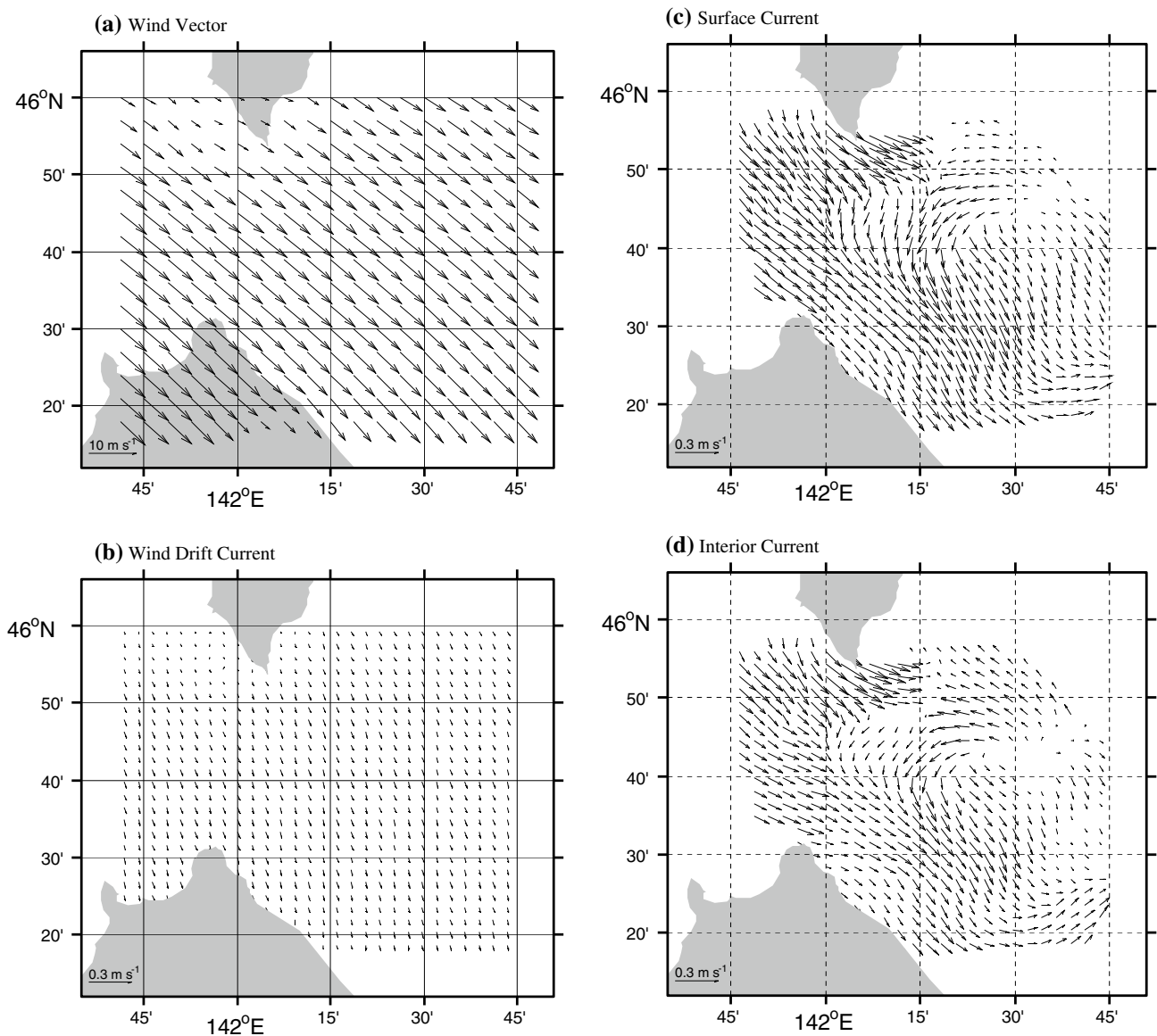


Fig. 13 Spatial distribution of monthly-mean wind and currents around the Soya Strait in January 2008: **a** monthly-mean wind, **b** monthly-mean wind drift current estimated from wind with ensemble-mean drift parameters, **c** monthly-mean surface current observed

by the HF ocean radars, and **d** monthly-mean interior current after the removal of the wind drift current shown in **b** from the surface current shown in **c**. Note that the *scale* of the *arrows* in **a** is different from those in the other *panels*

least squares method (LSM) and complex empirical orthogonal function/principal component analysis (CEOF/PCA).

Monthly- and ensemble-mean wind drift parameters from the two independent methods are roughly identical to each other, suggesting the robustness of the estimations. The monthly-mean turning angles are 3°–64° for both methods (except for an apparent outlier in August 2007) and the speed factors are 0.29–1.29 % for the LSM and 0.57–1.97 % for the CEOF method. Possible reasons for this outlier are a small amount of data and the weak and unstable wind in summer. No significant seasonal

variations in the wind drift parameters were discernible. The ensemble-mean turning angle and speed factor, calculated from the entire dataset (except August 2007 data) by the LSM, are 28° and 0.66 %, respectively.

The wind drift currents estimated from wind with the monthly- and ensemble-mean wind drift parameters are mostly consistent. They are southeastward and strong in fall and early winter, while being northwestward and weak in spring and early summer, mostly reflecting wind variations in this region. This result indicates that the use of the ensemble-mean wind drift parameters is a succinct and



Fig. 14 Monthly ratio between the wind drift current estimated using the ensemble-mean wind drift parameters and the interior current observed by the HF radars over an area within 50 km off the coast

effective way to estimate the wind drift current in the Soya Strait. The magnitude of wind drift current reaches 45 % of the interior current speed in winter and nearly 20 % in summer, indicating the importance of wind drift current estimation in this region. The removal of the wind drift current from the surface currents observed by the HF radars significantly improved the correlation between the SWC along-shore velocity and the sea level difference between Wakkanai and Abashiri. In the Soya Strait, the HF ocean radar system has continuously monitored the SWC since 2003. The wind drift parameters estimated in this study will help to correct the wind drift current component for the data over a period longer than 10 years and help reveal temporal and spatial variations in the SWC more precisely. Furthermore, the estimation of wind drift current is an important step for an accurate estimation of the volume transport of the SWC to discuss the mass budget of the Japan Sea, considering that surface currents in all three major straits (Tsushima, Soya, and Tsugaru) are now monitored by the HF ocean radars.

Acknowledgments The authors would like to thank Humio Mitsudera, Kay I. Ohshima, Tomohiro Nakamura, and Hiroto Abe for their constructive comments. Thanks are extended to the captain and crew onboard the *R/V Hinode-Maru* of the Soya Fishery Cooperative Society for their help with the deployment and recovery of the bottom mount, and Masao Ishikawa and Toru Takatsuka for their help with the radar observation. The tide-gauge and meteorological data were downloaded from the website of the Japan Meteorological Agency (JMA). The hydrographic data in the Soya Strait were obtained from the Japan Oceanographic Data Center (JODC). The heat flux data in the Soya Strait were obtained from the J-OFURO2 project. The JMA GPV data were downloaded from the website of the Research Institute for Sustainable Humanosphere, Kyoto University. This work was supported by the China Scholarship Council (file no. 2011627130).

References

- Chereskin TK, Roemmich D (1991) A comparison of measured and wind-derived Ekman transport at 11°N in the Atlantic Ocean. *J Phys Oceanogr* 21:869–878
- Cushman-Roisin B (1994) Introduction to geophysical fluid dynamics. Prentice Hall College Div, Englewood Cliffs, p 320
- Ebuchi N, Fukamachi Y, Ohshima KI, Shirasawa K, Ishikawa M, Takatsuka T, Daibo T, Wakatsuchi M (2006) Observation of the Soya Warm Current using HF ocean radar. *J Oceanogr* 62:47–61
- Ebuchi N, Fukamachi Y, Ohshima KI, Wakatsuchi M (2009) Subinertial and seasonal variations in the Soya Warm Current revealed by HF ocean radars, coastal tide gauges, and bottom-mounted ADCP. *J Oceanogr* 65:31–43
- Fukamachi Y, Tanaka I, Ohshima KI, Ebuchi N, Mizuta G, Yoshida H, Takayanagi S, Wakatsuchi M (2008) Volume transport of the Soya Warm Current revealed by bottom-mounted ADCP and ocean-radar measurement. *J Oceanogr* 64:385–392
- Fukamachi Y, Ohshima KI, Ebuchi N, Bando T, Ono K, Sano M (2010) Volume transport in the Soya Strait during 2006–2008. *J Oceanogr* 66:685–696
- Hanawa K, Mitsudera H (1985) On the data processing of daily mean values of oceanographic data—note on the daily mean sea-level data. *Bull Coast Oceanogr* 23:79–87 (in Japanese)
- Hanawa K, Yoshikawa Y, Taneda T (1996) TOLEX-ADCP monitoring. *Geophys Res Lett* 23:2429–2432
- Ide Y, Yoshikawa Y (2015) Effects of diurnal cycle of surface heat flux on wind-driven flow. *J Oceanogr*. doi:10.1007/s10872-015-0328-y (in press)
- Matsuyama M, Wadaka M, Abe T, Aota M, Koike Y (2006) Current structure and volume transport of the Soya Warm Current in summer. *J Oceanogr* 62:197–205
- Nakanowatari T, Ohshima KI (2014) Coherent sea level variability in and around the Sea of Okhotsk. *Prog Oceanogr* 126:58–70
- Ohshima KI (1994) The flow system in the Sea of Japan caused by a sea level difference through shallow straits. *J Geophys Res* 99:9925–9940
- Price JF, Weller RA, Pinkel R (1986) Diurnal cycling: observations and models of the upper ocean response to diurnal heating, cooling, and wind mixing. *J Geophys Res* 91:8411–8427
- Price JF, Weller RA, Schudlich RR (1987) Wind-driven ocean currents and Ekman transport. *Science* 238:1534–1538
- Schudlich RR, Price JF (1998) Observations of seasonal variation in the Ekman layer. *J Phys Oceanogr* 28:1187–1204
- Steiger JH (1980) Tests for comparing elements of a correlation matrix. *Psychol Bull* 87:245–251
- Teague WJ, Hwang PA, Jacobs GA, Book JW, Perkins HT (2005) Transport variability across the Korea/Tsushima Strait and the Tsushima Island Wake. *Deep Sea Res II* 52:1784–1801
- Thompson RORY (1983) Low-pass filters to suppress inertial and tidal frequencies. *J Phys Oceanogr* 13:1077–1083
- Toba Y (1988) Similarity law of wind wave and the coupling process of the air and water turbulent boundary layers. *Fluid Dyn Res* 2:263–279
- Tokeshi R, Ichikawa K, Fujii S, Sato K, Kojima S (2007) Estimating the geostrophic velocity obtained by HF radar observations in the upstream area of the Kuroshio. *J Oceanogr* 63:711–720
- Tomita H, Kubota M, Cronin MF, Iwasaki S, Konda M, Ichikawa H (2010) An assessment of surface heat fluxes from J-OFURO2 at the KEO and JKEO sites. *J Geophys Res* 115:C03018
- Weller RA (1981) Observations of the velocity response to wind forcing in the upper ocean. *J Geophys Res* 86:1969–1977
- Yoshikawa Y, Masuda A (2009) Seasonal variations in the speed factor and deflection angle of the wind-driven surface flow in the Tsushima Strait. *J Geophys Res* 114:C12022

Yoshikawa Y, Matsuno T, Marubayashi K, Fukudome K (2007) A surface velocity spiral observed with ADCP and HF radar in the Tsushima Strait. *J Geophys Res* 112:C06022

Yoshikawa Y, Masuda A, Marubayashi K, Ishibashi M (2010) Seasonal variations of the surface currents in the Tsushima Strait. *J Oceanogr* 66:223–232